

HybridSDF: Combining Free Form Shapes and Geometric Primitives for effective Shape Manipulation

Subeesh Vasu,¹ Nicolas Talabot,¹ Artem Lukoianov,² Pierre Baque,² Jonathan Donier,²
Pascal Fua¹

¹ CVLab, EPFL, Lausanne, Switzerland, firstname.lastname@epfl.ch

² Neural Concept SA, firstname.lastname@neuralconcept.com

Abstract

CAD modeling typically involves the use of simple geometric primitives whereas recent advances in deep-learning based 3D surface modeling have opened new shape design avenues. Unfortunately, these advances have not yet been accepted by the CAD community because they cannot be integrated into engineering workflows. To remedy this, we propose a novel approach to effectively combining geometric primitives and free-form surfaces represented by implicit surfaces for accurate modeling that preserves interpretability, enforces consistency, and enables easy manipulation.

1 Introduction

Most primitive-based approaches to CAD modeling rely on decomposing objects into parts represented by simple geometric shapes. Even though there has been intense interest in developing more sophisticated primitives (Hao et al. 2020; Deng et al. 2020; Kluger et al. 2021; Paschalidou et al. 2021), the accuracy and interpretability of the resulting models remains limited. In parallel, implicit surface representations (Sethian 1999), have recently re-emerged in the form of signed distance functions (Park et al. 2019) or occupancy fields (Mescheder et al. 2019; Chen and Zhang 2019) that can be implemented by deep networks that map 3D points to implicit function values. These representations are lightweight, high-fidelity, unlimited in resolution, naturally able to handle topology changes, and consequently extremely popular in the fields of computer vision and computer graphics. However, they have not yet been accepted by the CAD community because their implicit parameterization nature prevents them from being easily integrated into engineering workflows.

To change this, we propose a novel approach to effectively combining geometric primitives and free-form surfaces for accurate modeling that preserves interpretability, enforces consistency, and enables easy manipulation. To this end, we rely on three primitive types:

1. Simple geometric primitives, such as spheres and cylinders.
2. Primitives that bear a close resemblance to the simple ones but can deviate from them, such as the car wheels

Copyright © 2022, Association for the Advancement of Artificial Intelligence (www.aaai.org). All rights reserved.

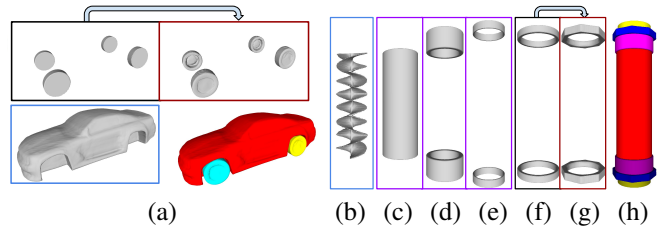


Figure 1: **Modeling complex objects.** (a) We depict cars as the combination of a main body and the wheels. The car body is represented by a *Generic SDF* (red) whose shape can change significantly. By contrast, the wheels are modeled by *Primitive-assisted-SDFs* (cyan and yellow) whose shape is constrained not to differ excessively from that of the cylindrical *Primitive-SDFs* shown in the upper left corner. (b-g). This depicts a static water-mixer. It comprises a spiral helix (b) whose shape can also change significantly and is represented by a *Generic SDF*. It is encased in a hollow-tube (c, red in h) with screws at both ends. The center tube along with the tube-like parts associated with the screw (d,e, yellow and violet in h) are represented by *Primitive-SDFs*. The screws also contains deformable rings modeled by *Primitive-assisted-SDFs* (g, blue in h) constrained not to deviate much from hollow tubes (f).

that are not quite cylinders.

3. Free form primitives that have arbitrarily complex shapes.

These three kinds of primitives are all represented by Signed Distance Functions (SDFs) that we will refer to as *primitive-SDFs*, *primitive-assisted-SDFs*, and *generic SDFs*. Fig. 1 depicts their respective roles. Their parameters are expressed in terms of latent vectors that can contain both explicit parameters, such as the radius and width of wheels, and implicit ones that are decoded together with the explicit parameters into 3D shapes.

This gives to designers the flexibility to represent parts that are true geometric primitives as such, parts that are similar but not identical by assisted primitives, and the remaining ones as free-form surfaces. As a result, our models are interpretable in terms of parts that can actually be manufactured unlike those of (Hao et al. 2020; Paschalidou et al. 2021) at no loss of accuracy. In short, our contribution is a novel SDF-based model that effectively combines the different kinds of primitives that are used in CAD to produce inter-

pretable models that retain their internal consistency when modified and are made of parts that can actually be built. This opens up new ways to perform 3D shape manipulations in a user-friendly manner, as we will demonstrate on the complex objects shown in Fig. 1.

2 Related Work

CAD models typically rely on simple geometric primitives. In recent years, the emergence of deep-learning has fostered an intense interest in developing more sophisticated primitives along with new ways to represent free form surfaces and to combine these two kinds of approaches. We review them briefly below.

2.1 Primitive-Based Representations

Existing primitive-based methods for 3D shape representation aim to derive interesting abstractions by decomposing the 3D shapes into semantically meaningful simpler parts. In addition to simple primitives, more sophisticated ones such as cuboids (Tulsiani et al. 2017; Zou et al. 2017; Niu, Li, and Xu 2018; Sun et al. 2019; Kluger et al. 2021), superquadrics (Paschalidou, Ulusoy, and Geiger 2019; Paschalidou, Gool, and Geiger 2020), anisotropic Gaussians (Genova et al. 2019), or convexes (Deng et al. 2020) have been proposed. All these works rely on a single primitive type to represent the entire shape. Hence, for complex shapes, reconstruction accuracy directly depends on the number of primitives used. To improve on this, the approach of (Paschalidou et al. 2021) defines a bijective function between traditional spherical primitives and a corresponding set of deformed shapes that can be arbitrarily complex.

As far as shape representation and shape manipulation are concerned, these deep learning-based methods have many limitations. They are typically trained in an unsupervised way to yield self-discovered arrangements of parts that do not necessarily correspond to semantically meaningful ones. Typically, the more primitives are used the more severe the problem becomes. For example, in (Paschalidou et al. 2021), the latent space is parameterized by sphere parameters that have no direct correspondence to the geometric parameters of the corresponding parts. Thus, there is no correspondence between the latent parameters and true geometric parameters, such as location, orientation, or size, which is something we provide and that a user can modify at will.

2.2 Explicit and Implicit Surfaces

Among existing 3D surface representations, meshes made of vertices and faces are one of the most popular and versatile types. There are excellent meshing algorithms (Peters and Reif 2008) that can refine a mesh so that it accurately represents a known 3D shape, but there are far fewer that can produce a detailed 3D mesh of an initially unknown 3D shape or an arbitrary topology. There have been many early attempts using only 3D meshes (Mcinerney and Terzopoulos 1999), but they require *ad hoc* heuristics that do not generalize well.

An alternative to surface meshes is to use an implicit description where the surface is described by the zero crossings

of a volumetric function $\Psi_{\mathbf{p}} : \mathbb{R}^3 \rightarrow \mathbb{R}$ that evolves over time (Sethian 1999). The strength of this implicit representation is that the zero-crossing surface can change topology without explicit re-parameterization. Until recently, its main drawback was thought to be that working with volumes, instead of surfaces, massively increased the computational burden. This changed dramatically with the introduction of continuous deep implicit-fields. They represent 3D shapes as level sets of deep networks that map 3D coordinates to a signed distance function (Park et al. 2019) or an occupancy field (Mescheder et al. 2019; Chen and Zhang 2019). This mapping yields a continuous shape representation that is lightweight but not limited in resolution. This representation has been successfully used for single-view reconstruction (Mescheder et al. 2019; Chen and Zhang 2019; Xu et al. 2019) and 3D shape-completion (Chibane, Alldieck, and Pons-Moll 2020). It has also been shown (Remelli et al. 2020; Guillard et al. 2021a) that 3D meshes could be extracted from these implicit representations without compromising differentiability. This makes it possible to simultaneously use explicit and implicit representations as needed, such as when optimizing a 3D shape so that its projections match a specific contour (Guillard et al. 2021b) or to maximize its aerodynamic performance. Recent works (Peng et al. 2020; Ibing, Lim, and Kobbelt 2021; Liu et al. 2021) have further extended the scope of implicit representations by developing network models that can yield fine-grained reconstruction of shapes.

2.3 Hybrid Representations

Hybrid methods attempt to combine different representations to yield enhanced benefits or additional functionalities. One common trend is to use a shared latent space across different representations such as voxel-based, image-based, or point-based representations to enhance performance in discriminative tasks such as classification and segmentation (Hegde and Zadeh 2016; Chen and Zhang 2019; Muralikrishnan et al. 2019). However, the *DualSDF* approach of (Hao et al. 2020) is the only other approach we know of that relies on a hybrid representation for shape generation and manipulation. It builds a shared latent space for two distinct shape representations, a sphere-based approximation and an implicit function-based high-fidelity reconstruction. The shared latent space couples the two representations and, as a result, the fine-grained model can be manipulated by changing the parameters of the spheres. However as the method of (Paschalidou et al. 2021), *DualSDF* suffers from the limited interpretability of the spherical primitives that do not correspond to specific body parts, which is a key difference with our approach.

3 Approach

In this section, we first introduce our hybrid representation and then the network that allows us to decode and encode complex 3D shapes into and from it.

3.1 HybridSDF Representation

Signed Distance Functions (SDFs) are mappings that associate to points $\mathbf{p} \in \mathbb{R}^3$ a value in \mathbb{R} that specifies their

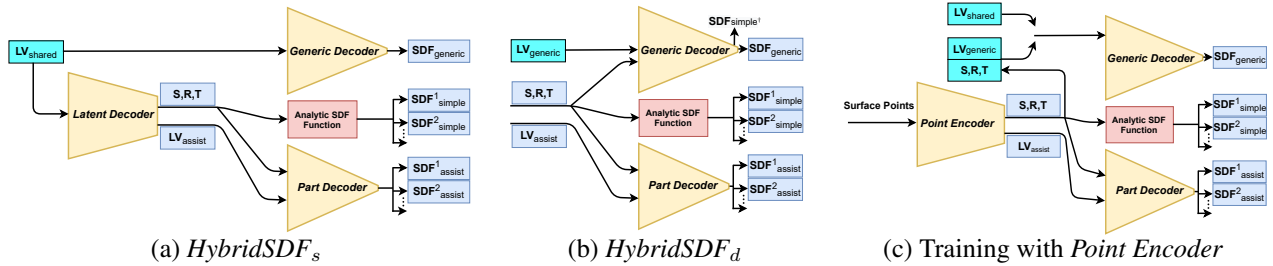


Figure 2: **Two architectures.** (a) $HybridSDF_s$ takes a single shared latent vector \mathbf{LV}_{shared} as input. It is decoded into an $SDF_{generic}$ and primitive parameters \mathbf{S} , \mathbf{R} , and \mathbf{T} along with an auxiliary latent vector \mathbf{LV}_{assist} , which are themselves decoded into the SDF_{simple}^j and SDF_{assist}^j . (b) By contrast, $HybridSDF_d$ takes as input \mathbf{S} , \mathbf{R} , \mathbf{T} , and \mathbf{LV}_{assist} along with a latent vector $\mathbf{LV}_{generic}$ that only encodes $SDF_{generic}$. (c) A *Point Encoder* takes as input the 3D point clouds from the training set and generates the \mathbf{S} , \mathbf{R} , \mathbf{T} , and \mathbf{LV}_{assist} values that are required for training purposes.

distance to the closest point on a closed surface. By convention, the value is negative if \mathbf{p} is inside the surface and positive otherwise. Hence, the surface is made of the zero crossings of the SDF. This representation allows the surfaces to change topology easily and differentiably, which can be exploited for shape optimization purposes. Furthermore, Boolean operators such as union and intersection that are traditionally used in constructive solid geometry can be implemented using min and max operations respectively on SDFs, which makes it easy to combine multiple ones into final shapes (Haugo, Stahl, and Brekke 2017). Hence, we represent the three kinds of primitives we use by the following SDFs.

- **Primitive-SDFs** (SDF_{simple}): These SDFs are parameterized by a small number of shape parameters (\mathbf{S}) that define where they are positive and negative. For example, the SDF of a cylinder is a function of its height and radius whereas hollow-cylinders require an inner and outer radius. To these one must add the rotation (\mathbf{R}) and translation (\mathbf{T}) parameters that define their 3D pose.
- **Primitive-assisted-SDFs** (SDF_{assist}): These SDFs can take arbitrary values but are constrained to not be too different from those of SDF_{simple} ones, which are defined by their own \mathbf{S} , \mathbf{R} , and \mathbf{T} parameters.
- **Generic SDFs** ($SDF_{generic}$): These are generic differentiable SDFs that can describe arbitrarily complex shapes.

They are depicted by Fig. 1. The complete shape is then taken to be a zero crossing of

$$SDF_{full} = \min(SDF_{simple}, SDF_{assist}, SDF_{generic}), \quad (1)$$

where

$$SDF_{simple} = \min(SDF_{simple}^1, \dots, SDF_{simple}^{n_s}),$$

$$SDF_{assist} = \min(SDF_{assist}^1, \dots, SDF_{assist}^{n_a}),$$

and n_s and n_a are the number of simple and assisted primitives, respectively.

3.2 Network Architectures

Our approach comes in two flavors, which we dub $HybridSDF_s$ and $HybridSDF_d$. The first relies on the same concept of shared latent space as *DeepSDF* (Park et al. 2019)

and *DualSDF* and, like them, is best suited for situations in which one wishes to change the shape locally and expects the the entire shape to change accordingly. The second is geared towards typical CAD applications that give the user control both over individual primitives and over the shape of the free-form surfaces. We describe them below in more details.

Shared Latent Vector ($HybridSDF_s$). In this version, we use a shared latent space that encodes the parameters of all three kinds of primitives without any component of the latent vector having a specific meaning. As shown in Fig. 2(a), such a vector \mathbf{LV}_{shared} is decoded both into a $SDF_{generic}$ and into the \mathbf{S} , \mathbf{R} , and \mathbf{T} geometric parameters, along with the auxiliary latent vector \mathbf{LV}_{assist} , which jointly define SDF_{simple} and SDF_{assist} . This is done by a *Latent Decoder* that comprises a single fully connected layer that extracts primitive-specific features followed by multiple independent branches of fully connected layers and non-linearities.

To generate SDF_{simple} from \mathbf{S} , \mathbf{R} , and \mathbf{T} , we rely on simple analytic functions that do not have to be learned. By contrast, to generate the SDF_{assist} from \mathbf{S} , \mathbf{R} , \mathbf{T} , and \mathbf{LV}_{assist} , we need a *Part Decoder*. It is also similar to that of *DeepSDF* but with only three layers because it only has to produce simpler shapes.

In practice, we take the latent vector \mathbf{LV}_{shared} to be of size 256 and the individual latent vectors \mathbf{LV}_{assist}^j to be of size 8. Similarly shaped parts, such as the wheels of the car and the screws of the mixer of Fig. 1, can share these latent vectors thus reducing the size of their concatenation \mathbf{LV}_{assist} .

Disentangled Latent Vector ($HybridSDF_d$). In this version depicted by Fig. 2(b), the network expects separate latent vectors $\mathbf{LV}_{generic}$ and \mathbf{LV}_{assist} that are used exclusively to produce $SDF_{generic}$ and SDF_{assist} , respectively. It also takes as input the geometric parameters \mathbf{S} , \mathbf{R} , and \mathbf{T} , which allows a designer to manually set up them if so desired.

We again use *DeepSDF* to implement the *Generic Decoder* as for $HybridSDF_s$ but with one key modification: we also use it to predict SDF_{simple} . This forces the *Generic Decoder* to take into account the explicit geometric parameters and, hence, to model the strong dependency between them and the free form parameters.

As the *Generic Decoder* now takes as input both the latent vector $\mathbf{LV}_{\text{generic}}$ and the geometric parameters, we take the dimension of $\mathbf{LV}_{\text{generic}}$ to be 256 minus the number of geometric parameters so that the full input to the *Generic Decoder* is again of dimension 256, for a fair comparison between the two variants of our approach.

3.3 Training the Network

To supervise the training of *HybridSDF_s* and *HybridSDF_d* given a set of training shapes in the form of 3D meshes, we need values for the explicit parameters \mathbf{S} , \mathbf{R} , \mathbf{T} as well as for $\mathbf{LV}_{\text{assist}}$. To this end, we use the *Point Encoder* depicted in Fig. 2(c) and take point clouds obtained from the training surfaces as input. Its architecture is that of a PointNet (Qi et al. 2017) with fully connected layers and non-linearities that independently predicts the individual primitive parameters \mathbf{S}^j , \mathbf{R}^j , \mathbf{T}^j , and $\mathbf{LV}_{\text{assist}}^j$. The latter are of a dimension 8 in all our experiments. All these vectors are then concatenated to form \mathbf{S} , \mathbf{R} , \mathbf{T} , and $\mathbf{LV}_{\text{assist}}$. During training the point-encoder is trained jointly with everything else as shown in Fig. 2(c). We can now define the training losses we minimize.

Common Loss. To train both *HybridSDF_s* and *HybridSDF_d*, we use a weighted sum of the following losses.

Reconstruction Losses. Minimizing reconstruction losses makes the predicted SDFs as close as possible to the ground-truth (GT) ones. We introduce two such losses, \mathcal{L}_r^f for the full object and \mathcal{L}_r^p for individual parts.

For the whole object, we write

$$\mathcal{L}_r^f = \frac{1}{K} \left\| \left\| \mathbf{SDF}_{\text{full}} - \mathbf{SDF}_{\text{full}}^{\text{GT}} \right\|_1 \right\|, \quad (2)$$

as in *DeepSDF*, where $\mathbf{SDF}_{\text{full}}^{\text{GT}}$ is the GT SDF and the L_1 norm is computed over K sample points.

To ensure that the primitives model the appropriate object parts, we build a robust version of the reconstruction loss for individual parts. To this end, we use part labels of the mesh to construct SDF samples for each part associated to a geometric primitive. We will refer to them as $\mathbf{SDF}_{\text{part}}^{\text{GT}}$. In practice, not only are the part labels available only for few shapes but they can also be extremely noisy. To mitigate, we define the robust loss function

$$\mathcal{L}_r^p = \frac{1}{\gamma K} \sum_{l=1}^{\gamma K} \text{Sort} \left\{ \left\| \mathbf{SDF}_{\text{part}} - \mathbf{SDF}_{\text{part}}^{\text{GT}} \right\|_l \right\} \quad (3)$$

where $\left\| \cdot \right\|_l$ indicates the absolute value, $\mathbf{SDF}_{\text{part}}$ is the predicted SDF of parts that can be a combination of geometric primitives and assisted ones, γ is a robustness factor having value ranging from 0 to 1, and *Sort* rearrange the sampled prediction errors in the increasing order of values. In other words, we average the lowest γK values of the errors.

In practice, we use both \mathcal{L}_r^f and \mathcal{L}_r^p for objects for which we have part labels, and only \mathcal{L}_r^f for the others.

Primitive Assistance. To force the primitive-assisted SDFs to resemble their corresponding geometric SDFs, we introduce

$$\mathcal{L}_{pa} = \frac{1}{K n_a} \sum_{n=1}^{n_a} \left\| \left\| \mathbf{SDF}_{\text{assist}}^n - \mathbf{SDF}_{\text{simple}}^{n+n_s} \right\|_1 \right\|, \quad (4)$$

where $\mathbf{SDF}_{\text{simple}}^n \Big|_{n=n_s+1}^{n_s+n_a}$ are the n_a geometric primitives used to assist $\mathbf{SDF}_{\text{assist}}^n \Big|_{n=1}^{n_a}$.

Intersection Loss. To prevent primitives from overlapping, we minimize an intersection loss between all pairs of primitives

$$\mathcal{L}_{ic} = \frac{1}{|x, y| K} \sum_{x, y} \left\| \left\| \mathcal{L}_{ov}(\mathbf{SDF}_x, \mathbf{SDF}_y) \right\|_1 \right\|, \quad (5)$$

$$\mathcal{L}_{ov}(\mathbf{SDF}_x, \mathbf{SDF}_y) = \max \left\{ -\max \{ \mathbf{SDF}_x, \mathbf{SDF}_y \}, 0 \right\},$$

where \mathcal{L}_{ov} is the overlap between \mathbf{SDF}_x and \mathbf{SDF}_y and $|x, y|$ the total number of such pairs.

Regularization Loss. To regularize the latent vectors, we also compute L_2 regularization losses on $\mathbf{LV}_{\text{assist}}$, $\mathbf{LV}_{\text{generic}}$, and $\mathbf{LV}_{\text{shared}}$, as in *DeepSDF*. We refer to the sum of all these L_2 losses as \mathcal{L}_{reg} .

Weighted Sum. Finally, these losses are summed into

$$\mathcal{L}_{\text{common}} = \mathcal{L}_r^f + \mathcal{L}_r^p + \lambda_{pa} \mathcal{L}_{pa} + \lambda_{ic} \mathcal{L}_{ic} + \lambda_{reg} \mathcal{L}_{reg}, \quad (6)$$

which we compute for both *HybridSDF_s* and *HybridSDF_d*.

Method Specific Losses. To $\mathcal{L}_{\text{common}}$, we add additional loss terms that are specific to *HybridSDF_s* or *HybridSDF_d*.

Recall that *HybridSDF_s* uses a *Latent Decoder* that predicts all the primitive parameters from the shared latent code. To supervise this prediction, we encourage similar SDF outputs using either the parameters from the *Point Encoder* or that of the *Latent Decoder* by introducing

$$\mathcal{L}_{\text{shared}} = \frac{1}{K(2n_a + n_s)} \left(\sum_{n=1}^{n_s+n_a} \left\| \left\| \mathbf{SDF}_{\text{simple}^*}^n - \mathbf{SDF}_{\text{simple}}^n \right\|_1 \right\| + \sum_{n=1}^{n_a} \left\| \left\| \mathbf{SDF}_{\text{assist}^*}^n - \mathbf{SDF}_{\text{assist}}^n \right\|_1 \right\| \right), \quad (7)$$

where $*$ denotes the SDF predictions derived from the output of the *Latent Decoder*.

For *HybridSDF_d*, we introduce instead

$$\mathcal{L}_{\text{dis}} = \frac{1}{K} \left\| \left\| \mathbf{SDF}_{\text{simple}^\dagger} - \min_{n=1}^{n_s+n_a} \mathbf{SDF}_{\text{simple}}^n \right\|_1 \right\|, \quad (8)$$

where $\mathbf{SDF}_{\text{simple}^\dagger}$ denotes the auxiliary output coming out of *Generic Decoder* as shown in Fig. 2(b). Minimizing it ensures that the *Generic Decoder* prediction $\mathbf{SDF}_{\text{generic}}$ is strongly dependent on the input explicit parameters.

4 Experiments

Our approach is designed to provide accurate reconstructions that can be easily edited and modified. We demonstrate these two facets of our work below and provide additional results and an ablation study in the supplementary material.

4.1 Datasets

We have experimented with two kinds of objects, the *Static Mixers* and *Cars* of Fig. 1. In both cases, we generate the training and test data using the same sampling strategy as in (Park et al. 2019). For the shapes that have part labels, we generate SDF samples for the part meshes as well. We use 10000 points sampled from the surface of full meshes as the input to the *Point Encoder* of Fig. 2(c)

Cars. We represent the cars from the publicly available ShapeNet dataset (Chang et al. 2015) in terms of a primitive-assisted-SDF for each wheel and a generic-SDF for the car body, as shown in Fig. 1(a). We obtained the wheel parameters from the noisy mesh labels of (Kalogerakis et al. 2017). This gave us 2283 training shapes, 247 of which have part labels, and 500 test shapes.

Static Mixers. They are used to mix liquids/gases/powders that have different chemical compositions, velocities, and temperatures. They comprise an internal part called a helix that is encased in a central tube, with screws at both ends, as shown in Fig. 1(h). It is natural to represent the central tube and the tube-like parts associated with the screw by primitive-SDFs, the screw ring by a primitive-assisted-SDF, and the helix whose shape can vary most from one mixer to another by a generic-SDF.

Our training set features three different types of helixes, and within each type the number of turns and point at which the helix starts varies. We provide examples in the supplementary material. Different mixers can vary in length and width. The total number of training and test shapes used for mixers are 1500 and 450, respectively. During training, we use part labels of tube and screw for 100 of the exemplars.

4.2 Baselines

We compare against the following state-of-the-art methods that are briefly described in Section 2:

- *DeepSDF* (Park et al. 2019): Auto-decoding network that predicts SDF of shapes from embedded latent codes.
- *HierSQ* (Paschalidou, Gool, and Geiger 2020): State-of-the-art primitive-only reconstruction that uses superquadrics.
- *NeuralParts* (Paschalidou et al. 2021): State-of-the-art primitive-only reconstruction that uses network-predicted primitives to improve fidelity.
- *DualSDF* (Hao et al. 2020): State-of-the-art hybrid approach to shape manipulation.

For all the above baselines, we used the code provided by the authors and we trained their networks on our data. We provide quantitative comparisons against both *HybridSDF_s* and *HybridSDF_d* and qualitative results using *HybridSDF_s*. We provide more such comparisons and results using *HybridSDF_d* in the supplementary material.

	Mixers			Cars		
	CD	EMD	sIoU	CD	EMD	sIoU
<i>DeepSDF</i>	2.27	2.76	86.3	11.9	1.44	54.9
<i>DualSDF</i>	4.56	3.17	77.8	17.4	1.88	49.1
<i>HierSQ</i>	19.6	7.03	28.3	27.8	2.63	36.8
<i>NeuralParts</i>	6.43	13.8	44.1	25	2.17	40
<i>HybridSDF_s</i>	1.61	2.49	90.2	13.6	1.46	52.9
<i>HybridSDF_d</i>	1.57	2.51	90.9	12.5	1.48	52.9

Table 1: Reconstruction results on the test sets of the Mixer and Car datasets. We report CD (30,000 points) multiplied by 10^4 , EMD (10,000 points) multiplied by 10^2 , and sIoU.

4.3 Shape Reconstruction

We trained our networks using the Adam optimizer (Kingma and Ba 2015) with a learning rate of $5e^{-4}$ for body decoder, $1e^{-3}$ for shared/body latent code, and $2e^{-4}$ for *Point Encoder*, *Latent Decoder*, and *Part Decoder*. We set the batch size to 32, use $K = 2000$ samples, and train all networks jointly for 2000 epochs. For the training loss in Eq. 6, we use the empirically found values $\lambda_{pa} = 0.1$, $\lambda_{ic} = 5$, and $\lambda_{reg} = 1e^{-4}$. The value of λ_{pa} controls the level of similarity between the geometric primitives and the assisted ones. A high weight will force the primitive assisted parts to become identical to the geometric primitives, while a very low value can allow the part-decoder to predict parts that are too different from the geometric primitives. A very high value of λ_{ic} can introduce undesired gaps between adjacent primitives whereas too low a value will fail to prevent overlaps. We illustrate this behavior in the supplementary material. For λ_{reg} , we use the values as in *DeepSDF*.

Fig. 3 depicts our reconstruction results on test shapes, as opposed to training shapes. Not only does our approach deliver visually appealing results, but it also captures geometric details that the other approaches can miss, such as the wheel orientation of the cars, without generating artifacts. In Table 1, we provide the corresponding quantitative results on the test sets in terms of Chamfer Distance l_2 (CD), Earth Mover’s Distance (EMD), and of shell-IoU (sIoU) as in (Remelli et al. 2020; Guillard, Remelli, and Fua 2020). sIoU is the intersection over union computed on voxelized surfaces of reconstructed and ground truth shapes, the higher its value the better. On the mixers, our approach yields the best accuracy. On the cars, *DeepSDF* does best and ours comes second, which is slightly counterintuitive given the qualitative mistakes *DeepSDF*, sometimes makes as shown in Fig. 3. We ascribe this to the fact that our learning task is harder. *HybridSDF_s* must produce two very different outputs, the generic SDF parameters and the explicit ones while the generic decoder of *HybridSDF_d* must similarly decode explicit and implicit parameters. Furthermore, *DeepSDF* uses all 256 degrees of freedom in the input latent vector to describe the shape, whereas our approach uses some of them to describe the geometric parameters, thus leaving a little less capacity for precise surface modeling. This is the price we pay for giving *HybridSDF_s* and *HybridSDF_d* the ability to manipulate shapes, which *DeepSDF* lacks and that we demonstrate below.

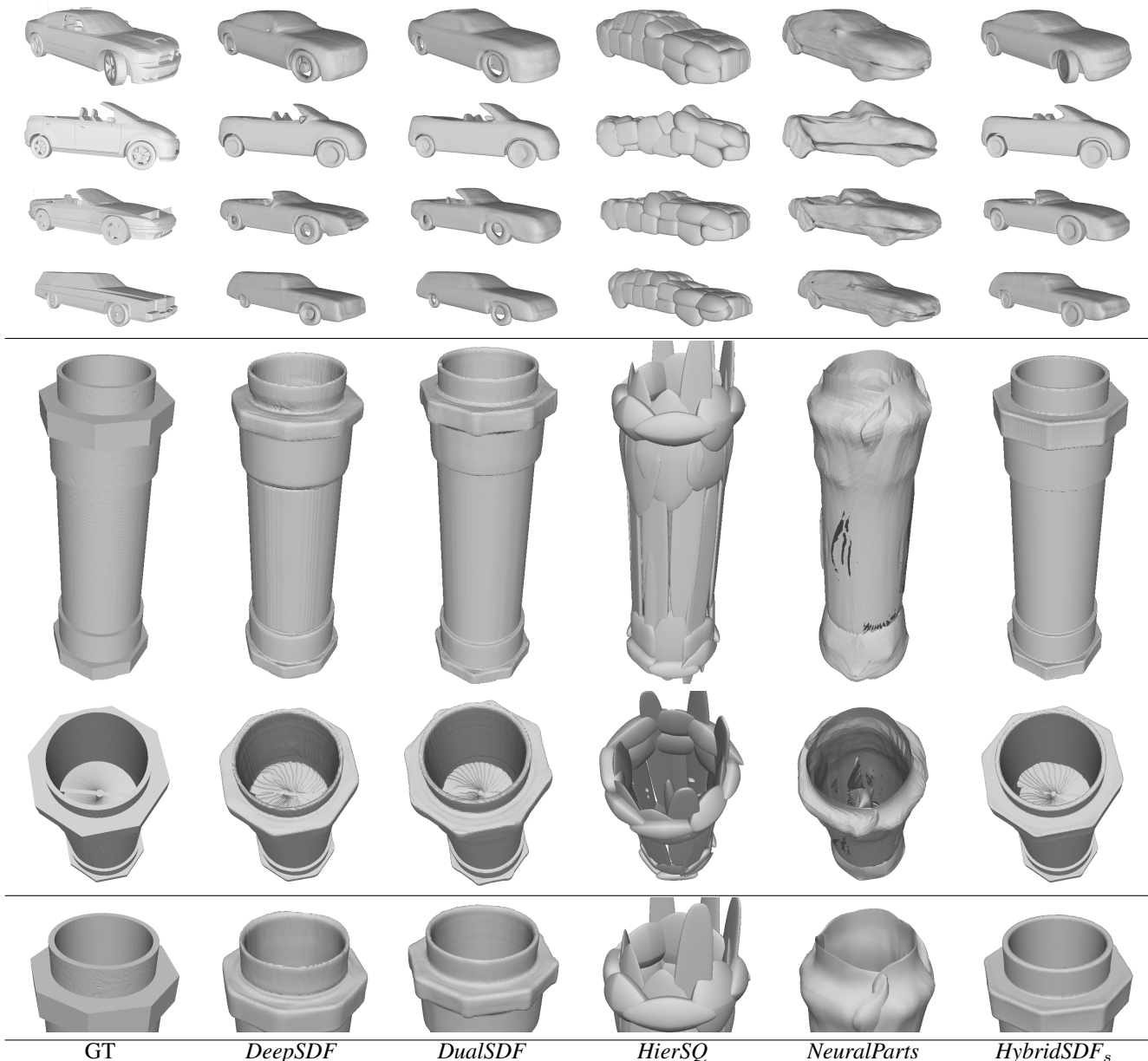


Figure 3: **Reconstruction results.** (Top Rows) Ground-truth for 4 different cars and corresponding reconstructions. *DeepSDF*, *DualSDF*, and *HybridSDF_s* deliver the most visually appealing results. However, *HybridSDF_s*, unlike *DeepSDF* and *DualSDF*, correctly captures the wheel orientation. (Bottom Rows) Ground-truth for 2 different mixers and reconstructions. The first one is seen from two different viewpoints. *DeepSDF*, *DualSDF*, and *HybridSDF_s* again yield the best looking results but both *DeepSDF* and *DualSDF* produce surface irregularities near the screw, while *HybridSDF_s* does not. Interestingly, *HierSQ* and *NeuralParts* completely fails to represent the helix, underscoring that iso-primitives are not the optimal way to represent shapes.

4.4 Shape Manipulation and Optimization

A key strength of our approach is its ability to perform interactive shape manipulation based on user-friendly inputs in the form of easily interpretable geometric parameters of parts such as, translation, rotation, and size. It can be employed to meet the requirements of two different CAD modeling use cases. *HybridSDF_s* is best when a user wishes to change a part of the object and expects the entire shape to change accordingly. By contrast, *HybridSDF_d* is most ap-

propriate when a user wants to change multiple parts of the object and have the remainder adapt. We discuss these two scenarios below.

Deforming one Part of the Object. In the shared representation of *HybridSDF_s*, all parts are tightly coupled. Hence, changing one will result in the entire shape adapting to that change. In the example of Fig. 4, we change the ring size of the mixer, that is, the radius of the hollow-cylinder

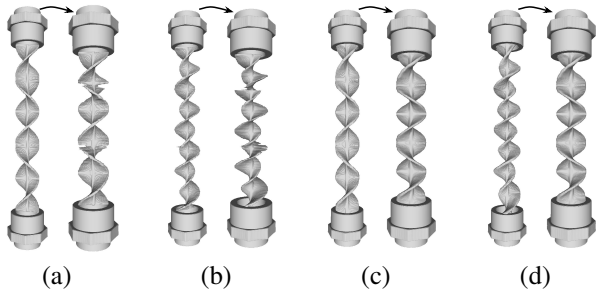


Figure 4: **Shape Manipulation using $HybridSDF_s$.** In each example we show two mixers, the source one on the left and the one obtained by changing the ring size. (a,b) Using $HybridSDF_s$. (c,d) Using $HybridSDF-V_s$.

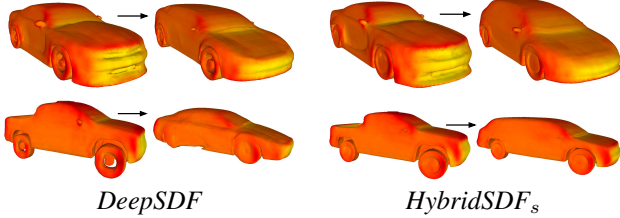


Figure 5: **Drag minimization.** We optimize two shapes generated by $DeepSDF$ and $HybridSDF_s$ to minimize the drag they incur. In all the examples, the initial shape is on the left and drag-optimized one on the right. The shapes are color coded from yellow for high pressure to red for low pressure.

that assists the ring reconstruction, by minimizing

$$\min_{\mathbf{LV}_{\text{shared}}} \left\| \mathcal{D}_l(\mathbf{LV}_{\text{shared}})^{ij} - V^* \right\|_1, \quad (9)$$

where \mathcal{D}_l refers to the *Latent Decoder*, (i, j) refers to the j^{th} parameter of i^{th} simple primitive chosen so that they are those of the rings, and V^* is the new target value for that parameter. As this only constrains the ring size, the other parts are free to undergo any deformation that is compatible with that value as shown in Fig. 4(a,b). If one wishes a more constrained deformation, we can replace the Generic Decoder $HybridSDF_s$ of by a Variational Auto-Decoder (VAD) (Hao et al. 2020). We dub this variant $HybridSDF-V_s$ and describe it in the supplementary material. It yields to a more regularized latent space, results are shown in Fig. 4(c,d).

The tight coupling between parts in a shared latent space also lends itself well to automated shape optimization as proposed in (Baqué et al. 2018; Remelli et al. 2020). Fig. 5 depicts two cars optimized for drag reduction in this manner. The resulting shapes are those of plausible cars whose wheels are still circular and do not touch the car body because $HybridSDF_s$ imposes these constraints. As shown in the supplementary material, $HybridSDF_s$ can also be integrated into the $DualSDF$ framework, resulting in an approach that also enforces these constraints while giving us the same real-time editing capability as in $DualSDF$.

Deforming Multiple Object Parts. In situations where the user can specify explicit values for *all* the geometric parameters, as in a CAD context, the disentangled representa-

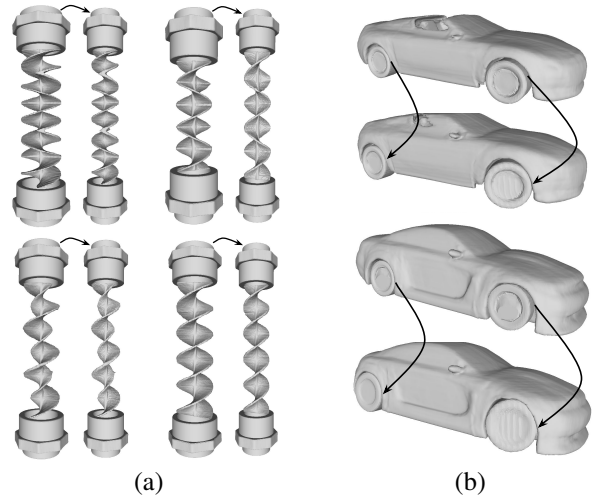


Figure 6: **Shape Manipulation using $HybridSDF_d$.** In each example, we again show a source object and the one obtained by changing some parameters. (a) For the mixers, we change all the explicit parameters, which causes proportionate changes of the helix and ring –source is on the left and results on the right. Unlike in the case of $HybridSDF_s$, the new helixes retain their original key features such as their type and number of turns. (b) For the cars, we change the position, orientation, and size of the wheels of the source shapes at the top and the body adapts accordingly, as shown at the bottom.

tion of $HybridSDF_d$ makes it possible to perform shape manipulation and to change multiple parts in an even simpler way. For example, Fig. 6 depicts the manipulation of mixers and cars by explicitly changing all these geometric parameters, that is, the size and orientation of the car wheels and the mixer ring sizes. The new geometric parameters \mathbf{S} , \mathbf{R} , and \mathbf{T} , along with the old latent vector $\mathbf{LV}_{\text{generic}}$, are fed to the Generic Decoder, resulting in a new $\mathbf{SDF}_{\text{generic}}$ that has adapted to the changed values. However, because this parameterization involves variables that are not commensurate, it is less well adapted to shape optimization as described above and $HybridSDF_s$ is better suited for that purpose.

5 Conclusion

We have proposed a novel approach to effectively combining geometric primitives and free-form surfaces represented by implicit surfaces for accurate modeling that preserves interpretability, enforces consistency, and enables easy manipulation of complex objects made of multiple parts. It comes in two flavors. One relies on a shared latent vector that allows manipulation of individual parts and global optimization. The other uses a disentangled representation that makes it easy to specify the geometric parameters of several parts and have the rest of the object adapt to these specifications.

In the current version of our architectures consistency between parts is enforced by minimizing loss functions. In future work, we will look into imposing such consistency constraints as hard constraints so that our loss functions have fewer terms and do not become needless complex as the number of parts increases.

References

- Baqué, P.; Remelli, E.; Fleuret, F.; and Fua, P. 2018. Geodesic Convolutional Shape Optimization. In *International Conference on Machine Learning*.
- Chang, A.; Funkhouser, T.; G., L.; Hanrahan, P.; Huang, Q.; Li, Z.; Savarese, S.; Savva, M.; Song, S.; Su, H.; Xiao, J.; Yi, L.; and Yu, F. 2015. Shapenet: An Information-Rich 3D Model Repository. In *arXiv Preprint*.
- Chen, Z.; and Zhang, H. 2019. Learning Implicit Fields for Generative Shape Modeling. In *Conference on Computer Vision and Pattern Recognition*.
- Chibane, J.; Alldieck, T.; and Pons-Moll, G. 2020. Implicit Functions in Feature Space for 3D Shape Reconstruction and Completion. In *Conference on Computer Vision and Pattern Recognition*.
- Deng, B.; Genova, K.; Yazdani, S.; Bouaziz, S.; Hinton, G.; and Tagliasacchi, A. 2020. Cvxnet: Learnable convex decomposition. In *Conference on Computer Vision and Pattern Recognition*, 31–44.
- Genova, K.; Cole, F.; Vlastic, D.; Sarna, A.; Freeman, W. T.; and Funkhouser, T. 2019. Learning Shape Templates with Structured Implicit Functions. In *International Conference on Computer Vision*, 7154–7164.
- Guillard, B.; Remelli, E.; and Fua, P. 2020. UCLID-Net: Single View Reconstruction in Object Space. In *Advances in Neural Information Processing Systems*.
- Guillard, B.; Remelli, E.; Lukoianov, A.; Richter, S.; Bagautdinov, T.; Baque, P.; and Fua, P. 2021a. DeepMesh: Differentiable Iso-Surface Extraction. *arXiv Preprint*.
- Guillard, B.; Remelli, E.; Yvernavy, P.; and Fua, P. 2021b. Sketch2Mesh: Reconstructing and Editing 3D Shapes from Sketches. In *International Conference on Computer Vision*.
- Hao, Z.; Averbuch-Elor, H.; Snavely, N.; and Belongie, S. 2020. Dualsdf: Semantic shape manipulation using a two-level representation. In *Conference on Computer Vision and Pattern Recognition*, 7631–7641.
- Haugo, S.; Stahl, A.; and Brekke, E. 2017. Continuous Signed Distance Functions for 3D Vision. In *International Conference on 3D Vision*, 116–125.
- Hegde, V.; and Zadeh, R. 2016. FusionNet: 3D Object Classification Using Multiple Data Representations. *CoRR*, abs/1607.05695.
- Ibing, M.; Lim, I.; and Kobbelt, L. 2021. 3D Shape Generation with Grid-based Implicit Functions. In *Conference on Computer Vision and Pattern Recognition*, 13559–13568.
- Kalogerakis, E.; Averkiou, M.; Maji, S.; and Chaudhuri, S. 2017. 3D shape segmentation with projective convolutional networks. In *Conference on Computer Vision and Pattern Recognition*, 3779–3788.
- Kingma, D. P.; and Ba, J. 2015. Adam: A Method for Stochastic Optimization. In *International Conference on Learning Representations*.
- Kluger, F.; Ackermann, H.; Brachmann, E.; Yang, M.; and Rosenhahn, B. 2021. Cuboids Revisited: Learning Robust 3D Shape Fitting to Single RGB Images. In *Conference on Computer Vision and Pattern Recognition*, 13070–13079.
- Liu, S.; Guo, H.; Pan, H.; Wang, P.; Tong, X.; and Liu, Y. 2021. Deep Implicit Moving Least-Squares Functions for 3D Reconstruction. In *Conference on Computer Vision and Pattern Recognition*, 1788–1797.
- Mcinerney, T.; and Terzopoulos, D. 1999. Topology Adaptive Deformable Surfaces for Medical Image Volume Segmentation. *IEEE Transactions on Medical Imaging*, 18(10): 840–850.
- Mescheder, L.; Oechsle, M.; Niemeyer, M.; Nowozin, S.; and Geiger, A. 2019. Occupancy Networks: Learning 3D Reconstruction in Function Space. In *Conference on Computer Vision and Pattern Recognition*, 4460–4470.
- Muralikrishnan, S.; Kim, V. G.; Fisher, M.; and Chaudhuri, S. 2019. Shape unicode: A unified shape representation. In *Conference on Computer Vision and Pattern Recognition*, 3790–3799.
- Niu, C.; Li, J.; and Xu, K. 2018. Im2struct: Recovering 3d shape structure from a single rgb image. In *Conference on Computer Vision and Pattern Recognition*, 4521–4529.
- Park, J. J.; Florence, P.; Straub, J.; Newcombe, R. A.; and Lovegrove, S. 2019. DeepSdf: Learning Continuous Signed Distance Functions for Shape Representation. In *Conference on Computer Vision and Pattern Recognition*.
- Paschalidou, D.; Gool, L. V.; and Geiger, A. 2020. Learning unsupervised hierarchical part decomposition of 3d objects from a single rgb image. In *Conference on Computer Vision and Pattern Recognition*, 1060–1070.
- Paschalidou, D.; Katharopoulos, A.; Geiger, A.; and Fidler, S. 2021. Neural Parts: Learning expressive 3D shape abstractions with invertible neural networks. In *Conference on Computer Vision and Pattern Recognition*, 3204–3215.
- Paschalidou, D.; Ulusoy, A. O.; and Geiger, A. 2019. Superquadrics revisited: Learning 3d shape parsing beyond cuboids. In *Conference on Computer Vision and Pattern Recognition*, 10344–10353.
- Peng, S.; Niemeyer, M.; Mescheder, L.; Pollefeys, M.; and Geiger, A. 2020. Convolutional Occupancy Networks. In *European Conference on Computer Vision*, 523–540.
- Peters, J.; and Reif, U. 2008. *Subdivision Surfaces*. Springer.
- Qi, C. R.; Su, H.; Mo, K.; and Guibas, L. J. 2017. Pointnet: Deep Learning on Point Sets for 3D Classification and Segmentation. In *Conference on Computer Vision and Pattern Recognition*.
- Remelli, E.; Lukoianov, A.; Richter, S.; Guillard, B.; Bagautdinov, T.; Baque, P.; and Fua, P. 2020. MeshSdf: Differentiable Iso-Surface Extraction. In *Advances in Neural Information Processing Systems*.
- Sethian, J. A. 1999. *Level Set Methods and Fast Marching Methods Evolving Interfaces in Computational Geometry, Fluid Mechanics, Computer Vision, and Materials Science*. Cambridge University Press.
- Sun, C.; Zou, Q.; Tong, X.; and Liu, Y. 2019. Learning adaptive hierarchical cuboid abstractions of 3d shape collections. *ACM Transactions on Graphics*, 38(6): 1–13.
- Tulsiani, S.; Su, H.; Guibas, L. J.; Efros, A. A.; and Malik, J. 2017. Learning shape abstractions by assembling volumetric

primitives. In *Conference on Computer Vision and Pattern Recognition*, 2635–2643.

Xu, Q.; Wang, W.; Ceylan, D.; Mech, R.; and Neumann, U. 2019. DISN: Deep Implicit Surface Network for High-Quality Single-View 3D Reconstruction. In *Advances in Neural Information Processing Systems*.

Zou, C.; Yumer, E.; Yang, J.; Ceylan, D.; and Hoiem, D. 2017. 3D-PRNN: Generating Shape Primitives with Recurrent Neural Networks. In *International Conference on Computer Vision*.